Am J Transl Res 2021;13(11):12480-12494
www.ajtr.org /ISSN:1943-8141/AJTR0106251

Original Article

Monoexponential, biexponential and stretched exponential models of diffusion weighted magnetic resonance imaging in glioma in relation to histopathologic grade and Ki-67 labeling index using high B values

Nabin Chaudhary, Guiling Zhang, Shihui Li, Wenzhen Zhu

Department of Radiology, Tongji Hospital, Tongji Medical College, Huazhong University of Science and Technology, No. 1095 Jiefang Avenue, Wuhan 430030, Hubei, China

Received December 11, 2019; Accepted March 12, 2021; Epub November 15, 2021; Published November 30, 2021

Abstract: Purpose: To explore the performance of various parameters obtained from monoexponential (Gaussian), biexponential and stretched exponential (non-Gaussian) models of Diffusion Weighted Magnetic Resonance Imaging in differentiating gliomas with correlation to histopathology and Ki-67 labeling index (LI). Materials and methods: This Institute Review Board approved retrospective study included 51 pathologically proven glioma patients (WHO Grade I, n = 1; Grade II, n = 19, Grade III, n = 12; Grade IV, n = 19), and immunohistochemistry for Ki-67 LI was obtained. The conventional Magnetic Resonance (MR) images and Diffusion Weighted (DW) images with 19 non-zero b values (0-4500 s/mm^2) followed by contrast-enhanced MR images were obtained at 3T preoperatively. All images were processed with Advantage Workstation 4.5 (GE Medical Systems). Region of interest (ROI) in the solid part of the tumor was manually drawn along the border meticulously excluding areas of edema, cyst, hemorrhage, necrosis, and/or calcification, and the parameters: Apparent Diffusion Coefficient (ADC) of monoexponential; pure molecular diffusion coefficient (Dslow), pseudo-diffusion coefficient (Dfast), and perfusion fraction (f) of biexponential; Distributed Diffusion Coefficient (DDC), and heterogeneity index (α) of stretched exponential models were obtained. ROI of 50 mm^2 in the contralateral normal appearing white matter (NAWM) was drawn for the internal control either on centrum semiovale or white matter of the frontal lobe. Analysis of reliability by Intra-class Correlation Coefficient (ICC); correlation with Ki-67 LI by Spearman's rank correlation; comparison between high grade glioma (HGG) and low grade glioma (LGG) by either Mann Whitney U test or Independent t-Test; comparison among Grade II, III and IV gliomas by one-way ANOVA with Bonferroni; and diagnostic performance by analysis of Area Under Receiver Operating Characteristic (ROC) Curve (AUC) were conducted. Results: Highly significant differences were found between HGG and LGG for all the parameters ($P < 0.001$ for all). In differentiating HGG from LGG, AUC values were 0.955 for Ki-67 LI; 0.926 for α; 0.903 for Dslow; 0.897 for f; 0.863 for DDC; 0.852 for ADC; 0.820 for Dfast ($P < 0.001$ for all). The parameters ADC, Dslow, Dfast, f, DDC, and α showed moderate to good negative correlation with Ki-67 LI ($P < 0.001$ for all). The ICCs of all the parameters were found greater than 0.75 ($P < 0.05$ for all) suggesting good reliability of measurements. Conclusion: In comparison to ADC derived from monoexponential model, the parameters α and Dslow derived from stretched exponential, and biexponential models respectively can efficiently differentiate HGG from LGG with high diagnostic accuracy. Additionally, f and DDC derived from biexponential, and stretched exponential models respectively are also more useful in differentiating HGG from LGG in comparison to ADC.

Keywords: Monoexponential model, biexponential model, stretched exponential model, glioma grade, Ki-67 labeling index, diffusion weighted MR imaging

Introduction

Gliomas are the most common group of primary malignant brain tumors with varying degree of heterogeneity. According to WHO, gliomas are divided into four histologic grades, Grade I to IV in the increasing order of aggressive biological behavior and poorer prognosis that serves as a guidance for deciding appropriate treatment strategy [1-3]. High grade gliomas

(HGGs: Grade III & IV) are usually treated with maximal surgical resection along with adjuvant radiotherapy and/or chemotherapy, whereas in low-grade gliomas (LGGs: Grade I & II), only maximal tumor resection is performed in most patients with vigilant follow up [4-7]. The prognosis of HGGs is poor in spite of aggressive therapy due to infiltrative nature and higher recurrence [1, 8, 9]. Therefore, accurate differentiation and grading is vital for proper treatment planning in order to improve the survival of the patients.

Histopathology is the reference standard for grading but suffers from inherent sampling bias and also requires assessment by an expert with potential limitations of inter and intra-observer variability [10-12]. Preoperative evaluation of glioma by advanced Magnetic Resonance Imaging (MRI) modalities improves the diagnostic yield as it can localize the tumor precisely, and also can provide non-invasive grading [13]. Imaging in glioma can play an important role, particularly Diffusion Weighted Magnetic Resonance Imaging (DW-MRI) as it has a great potential in accurately differentiating the glioma grade, and providing more insight into the cellularity and aggressiveness of the tumor, thereby help determine the optimal therapeutic approach and predict the most likely prognosis [9].

Various models of DW-MRI have been proposed so far in order to better explain the diffusion of water molecules in the biological tissues, thus enabling to efficiently image and reliably grade tumors like glioma. The conventional, also known as monoexponential model of DW-MRI assumes the Gaussian behavior or the displacement distribution of free water molecules in a homogeneous medium [14, 15]. However, various studies show deviation from this and emphasize non-Gaussian or anomalous diffusion of water molecules in the body tissues, namely biexponential model [16], and stretched exponential model [17], which attempt to provide better explanation of diffusion behavior of water molecules in a rather restricted and complex environment that suffers hindrance from inside, outside, around and through cellular structures. Biexponential model considers two separate compartments of water diffusion pools, intracellular and extracellular [16, 18, 19]. Stretched exponential model, on the other hand explains the diffusion heterogeneity across the tissue irrespective of number of compartments [17, 20].

Various studies have been carried out using these models to identify the relationship with the grade of glioma while very few have correlated them with Ki-67 labeling index (Ki-67 LI) [21, 22]. Ki-67 is an IgG1 class monoclonal antibody that recognizes a core antigen present in proliferating cells and absent in quiescent cells which is expressed in all phases of the cell cycle except G0 and early parts of G1 [23]. Ki-67 LI is the simplest and most reliable methods of all which has an excellent correlation with the grade of the tumor [11]. Furthermore, it is not dependent on factors such as age and sex [24]. The assessment of proliferative activity by means of Ki-67 immunostaining can supplement standard histological grading by providing important therapeutic and prognostic information [10, 11].

The aim of this study is to correlate both histopathologic grade of glioma and Ki-67 LI with various parameters obtained from monoexponential, biexponential, and stretched exponential models.

Materials and methods

Patient selection

This retrospective study was approved by Institute Review Board of Tongji Hospital and written informed consent of all patients was obtained. Out of 96 confirmed glioma patients by histopathology from February 2014 to February 2015, 45 were excluded due to reasons: (a) motion artifact or poor image quality, n = 2; (b) non-availability of Ki-67 LI, n = 9; and (c) not imaged with 19 non-zero multi b values, n = 34. The remaining 51 were included in the study, who underwent preoperative brain MRI at 3T on GE MR 750 system (GE Healthcare, Milwaukee, WI) with 19 non-zero multi b values (0, 20, 50, 80, 100, 150, 200, 400, 600, 800, 1000, 1200, 1500, 2000, 2400, 2800, 3200, 3600, 4000, 4500 s/mm^2), and underwent surgical resection. None were biopsied for pathological specimen. Immunohistochemistry was performed to obtain Ki-67 LI. Among these, 27 were males and 24 were females (mean age = 42; age range: 11-75 years; Grade I, n = 1,

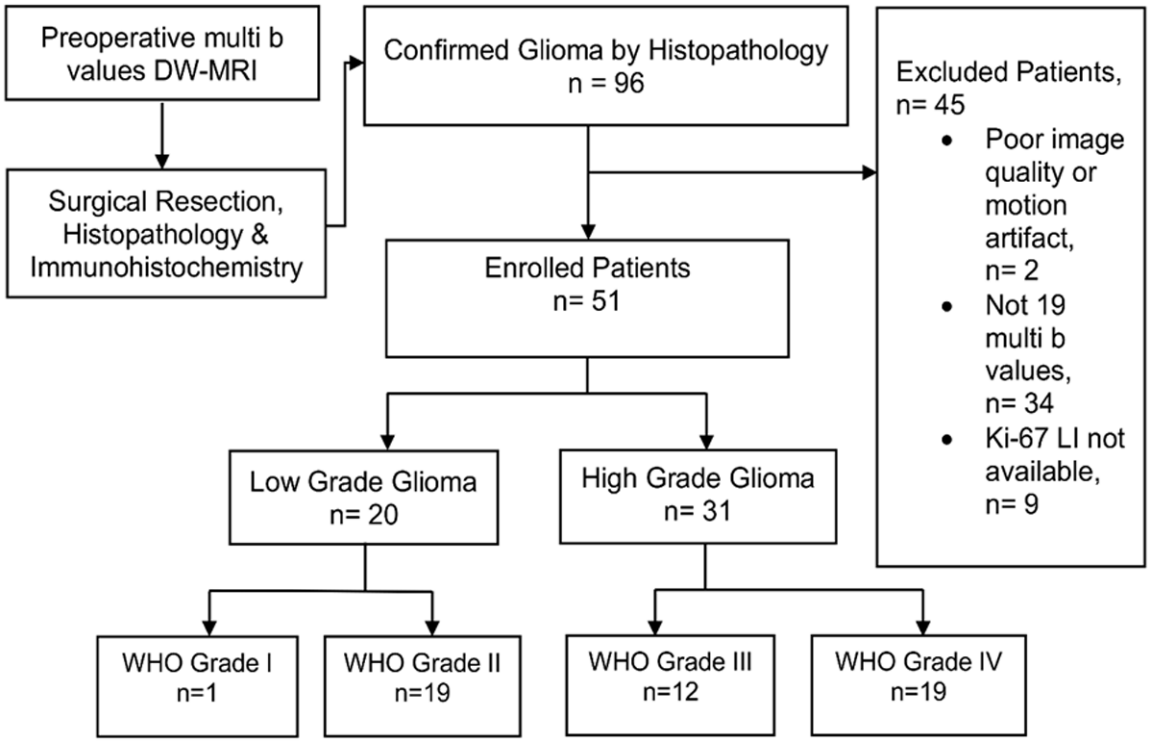

Figure 1. Flow chart of the study. Out of 96 confirmed glioma patients by histopathology, 45 were excluded due to reasons explained in the chart. The remaining 51 were included in the study which consisted of Low Grade Glioma, n = 20 (Grade I, n = 1, Grade II, n = 19), and High Grade Glioma, n = 31 (Grade III, n = 12, Grade IV, n = 19. These patients underwent brain MRI at 3T using 19 non-zero multi b values (0-4500 s/mm^2) prior to surgery. Immunohistochemistry was performed in surgical resection specimens of all patients to obtain Ki-67 LI. DW-MRI = Diffusion Weighted Magnetic Resonance Imaging, Ki-67 LI = Ki-67 Labeling Index.

Grade II, n = 19, Grade III, n = 12, Grade IV, n = 19). The maximum duration for surgery after MRI scan was 25 days. The flowchart of the study is depicted in **Figure 1**, and the detailed characteristics of the glioma patients is illustrated in **Table 1**.

Image acquisition

All MR images were obtained with a 3T MR system (MR 750, GE Healthcare, Milwaukee, WI, USA) with a 32-channel phased-array coil. The conventional MR images and DW images with 19 non-zero multi b values (0-4500 s/mm^2) followed by contrast-enhanced MR images were acquired during the same procedure.

The conventional MR scans included transverse T1 fluid-attenuated inversion recovery (T1-FLAIR), transverse T2 fast spin echo (T2-FSE) and transverse T2 fluid-attenuated inversion recovery (T2-FLAIR). The acquisition parameters applied were: TR = 2,992 ms, TE = 24 ms, TI = 869 ms, NEX = 1, matrix = 320 × 320 for T1-FLAIR; TR = 4,599 ms; TE = 102 ms; NEX = 2; matrix = 320 × 224 for T2-FSE; TR = 8,000 ms; TE = 160 ms; TI = 2,100 ms; NEX = 1; matrix = 256 × 256 for T2-FLAIR. The section thickness, spacing, section number and FOV of the sequences were 5 mm, 1.5 mm, 20 and 240 × 240 cm^2 respectively.

DWI images were acquired in axial planes with single-shot diffusion-weighted spin-echo echo-planar sequence (TR, 3,000 ms; TE, 70 ms; NEX, 4; matrix, 160 × 160; number of sections, 20; sections thickness, 5 mm; spacing, 1.5 mm; and FOV, 240 × 240 cm^2) applying 19 non-zero multi b values of 0, 20, 50, 80, 100, 150, 200, 400, 600, 800, 1000, 1200, 1500, 2000, 2400, 2800, 3200, 3600, 4000, 4500 s/mm^2.

Finally, contrast enhanced-T1 weighted images (CE-T1WI) were obtained. The scan plane was parallel to the line joining anterior and posterior commissure, and the range covered the entire brain.

Table 1. Characteristics of glioma patients

Characteristics	Value/No.
Age (years)	
Mean ± SD	41.92 ± 14.31
Median	46
Range	11-75
Sex	
Male	27
Female	24
Pathological specimen	
Surgical resection	51
Biopsy	0
Pathology	
LGG	20
Pilocytic astrocytoma, Grade I	1
Diffuse astrocytoma, Grade II	11
Oligodendroglioma, Grade II	5
Oligo-astrocytoma, Grade II	3
HGG	31
Anaplastic astrocytoma, Grade III	10
Anaplastic oligodendroglioma, Grade III	1
Anaplastic oligo-astrocytoma, Grade III	1
Glioblastoma, Grade IV	19

SD = Standard Deviation, No. = Number, LGG = Low Grade Glioma, HGG = High Grade Glioma.

Image processing and analysis

All images were obtained and transferred to a FUNCTOOL workstation (Advantage Workstation 4.5; GE Medical Systems) for processing and then evaluated by two different radiologists (N.C. and G. Z. with 5 and 3 years of experience respectively) independently while being blinded to the pathology. The average values were calculated for each of the parameters for data analysis and inter-observer reliability was assessed.

At first, the conventional and contrast-enhanced images were meticulously observed and the tumor size, location, enhancement pattern and the presence of edema, cyst, hemorrhage and/or necrosis were identified. In doubtful cases, the study guide (W.Z.) with more than 25 years of neuroradiology experience was consulted. Region of interest (ROI) in the solid part of the tumor was manually drawn along the margin carefully excluding areas of edema, cyst, hemorrhage, necrosis, and/or calcification. The mean tumor area examined was 244.49 mm^2. Similarly, ROI of 50 mm^2 in the contralateral normal appearing white matter (NAWM) was drawn for the internal control for which contralateral centrum semiovale was chosen, and in cases where this site was involved by the tumor, the contralateral white matter of the frontal lobe was considered. Various parameters by the different models using high multi b values were obtained. The equations of the models are as follows:

Monoexponential model:

$$\frac{S(b)}{S(0)} = \exp(-b.ADC) \quad (1)$$

Biexponential Model:

$$\frac{S(b)}{S(0)} = f.\exp(-b.Dfast) + (1-f).\exp(-b.Dslow) \quad (2)$$

Stretched exponential Model:

$$\frac{S(b)}{S(0)} = \exp[(-b.DDC)^{\alpha}] \quad (3)$$

Where, S(b) is the signal intensity at a particular b value, S(0) is the signal intensity at b = 0 s/mm^2, the diffusion sensitivity factor b is equal to $\gamma^2G^2d^2$ (D-d/3); γ is the gyromagnetic ratio, G is the magnitude of, δ is width of, and Δ is the time between two balanced diffusion weighted gradient pulses. ADC is the diffusion coefficient of the monoexponential model. Dfast, Dslow, f are the diffusion parameters of the biexponential model; Dfast, fast ADC is the pseudo-diffusion coefficient; Dslow is the pure molecular diffusion coefficient, and f is fraction of fast ADC (the perfusion fraction), and DDC is the diffusion coefficient of the stretched exponential model and α is the water diffusion heterogeneity index between 0 and 1. The mean and standard deviation of the parameters obtained are presented in **Table 2**.

Histopathology and Ki-67 labeling index

The solid areas of the tumor were identified by preoperative assessment of the MR images. The neurosurgeon was well informed prior to surgery to obtain the corresponding tissue during surgery for histopathological examination, thereby minimizing sampling bias. None of the patients were biopsied. The histologic grading of the tumor was determined based on WHO [1]. The updated 2016 classification has added

Table 2. Mean and standard deviation of the parameters

	ADC	Dslow	Dfast	f	DDC	α
Grade II (n = 19)	1.06 ± 0.26	0.75 ± 0.16	2.39 ± 0.32	0.73 ± 0.13	1.66 ± 0.54	0.92 ± 0.07
Grade III (n = 12)	0.81 ± 0.12	0.57 ± 0.10	2.71 ± 0.44	0.58 ± 0.13	1.08 ± 0.12	0.82 ± 0.05
Grade IV (n = 19)	0.68 ± 0.15	0.46 ± 0.70	3.10 ± 0.41	0.45 ± 0.10	0.88 ± 0.14	0.76 ± 0.04
LGG (n = 20)	1.07 ± 0.26	0.75 ± 0.16	2.43 ± 0.36	0.74 ± 0.14	1.69 ± 0.54	0.91 ± 0.06
HGG (n = 31)	0.73 ± 0.15	0.50 ± 0.10	2.95 ± 0.46	0.50 ± 0.13	0.96 ± 0.16	0.79 ± 0.05
NAWM (n = 51)	0.44 ± 0.03	0.33 ± 0.03	2.12 ± 0.21	0.38 ± 0.05	0.57 ± 0.08	0.73 ± 0.03

ADC (× 10^{-3} mm^2/s), Dslow (× 10^{-3} mm^2/s), Dfast (× 10^{-3} mm^2/s), f (unitless), DDC (× 10^{-3} mm^2/s), α (unitless), NAWM = Normal Appearing White Matter.

Table 3. Ki-67 Labeling Index (LI) in low and high grade gliomas

Ki-67 LI (%)	Mean	SD	Median	Minimum	Maximum
LGG (n = 20)	3.95	02.31	4.00	1.00	10.00
HGG (n = 31)	25.68	20.86	20.00	3.00	80.00

SD = Standard Deviation.

molecular and genetic information onto histologic grading to form final integrated diagnosis. However, the WHO grade basically remains the same which is solely based on microscopy/histopathology, and our study is limited to WHO histologic grading [2, 3].

Immuno-histochemical staining for Ki-67 LI was performed by the Envision method (Clone No. UMAB107, dilution 1:300). The tumor sections were quantified based on the percentage of positive cells in the highest density of the stained areas; all cells with nuclear staining of any intensity were considered positive, and the Ki-67 LI values were reported as the percentage of positive cells among the total cells counted [25]. The mean, standard deviation, median, minimum, and maximum values of Ki-67 LI in low and high grade gliomas are shown in **Table 3**.

Statistical analysis

Analysis of reliability: The reliability of ADC, Dslow, Dfast, f, DDC, and α was assessed by inter-observer reliability using the Intra-class Correlation Coefficient (ICC). The ICC was interpreted as poor if it was < 0.4, moderate if ≥ 0.4 but < 0.75, and as good if > 0.75 [26].

Tests of normality: The distribution of the various parameters obtained from the tumor area were assessed by Kolmogorov-Smirnov test.

Comparison between groups of HGG and LGG: The parameters which were normal in distribution in both groups were compared by Independent t-Test and those which did not follow normal distribution in either one group were compared by Mann-Whitney U Test.

Comparison among groups of Grade II, Grade III, and Grade IV: One-way ANOVA with Bonferroni (corrected *p* value of 0.0125) was used for multiple comparisons.

Correlation of parameters with Ki-67 LI: The Spearman's rank test was used to identify the correlation of ADC, Dslow, Dfast, f, DDC, and α with Ki-67 LI. The correlation coefficient rho (r) was categorized as little or fair ($0 \leq r \leq 0.4$), moderate to good ($0.4 < r \leq 0.75$), and very good to excellent ($0.75 < r$) [27].

ROC curve analysis: Receiver operating characteristic curve (ROC) analysis was performed to obtain the area under the receiver operating characteristic curve (AUC), and the cutoff value, sensitivity, and specificity to compare the diagnostic accuracy of the parameters. The most appropriate cutoff values were determined according to the greatest Youden index (also called Youden's J statistic, J = sensitivity + specificity - 1) from the estimated curves [28].

Numerical variables were expressed as the mean and standard deviation. The units used were ADC (× 10^{-3} mm^2/s); Dslow (× 10^{-3} mm^2/s); Dfast (× 10^{-3} mm^2/s); f (unitless); DDC (× 10^{-3} mm^2/s); α (unitless); and Ki-67 labeling index (%). All the statistical analyses were performed by IBM SPSS 23.0 software (IBM Corp, Chicago, IL, USA). A significant level of $P < 0.05$ was used for all the tests except for multiple comparisons among groups by one-way ANOVA with Bonferroni where corrected *p* value of 0.0125 was used. All the tests were two-tailed.

Table 4. The inter-observer reliability of the parameters in the tumor area

		ADC	Dslow	Dfast	f	DDC	α
Grade II (n = 19)	Observation 1	1.06 ± 0.25	0.75 ± 0.16	2.39 ± 0.35	0.74 ± 0.14	1.66 ± 0.53	0.92 ± 0.07
	Observation 2	1.05 ± 0.26	0.75 ± 0.16	2.38 ± 0.31	0.72 ± 0.14	1.65 ± 0.56	0.91 ± 0.07
	ICC	0.993	0.998	0.969	0.972	0.994	0.974
	p value	< 0.001	< 0.001	< 0.001	< 0.001	< 0.001	< 0.001
Grade III (n = 12)	Observation 1	0.82 ± 0.13	0.57 ± 0.10	2.70 ± 0.44	0.58 ± 0.13	1.10 ± 0.14	0.82 ± 0.05
	Observation 2	0.80 ± 0.12	0.57 ± 0.10	2.73 ± 0.44	0.58 ± 0.13	1.06 ± 0.11	0.83 ± 0.05
	ICC	0.990	0.989	0.987	0.994	0.886	0.986
	p value	< 0.001	< 0.001	< 0.001	< 0.001	< 0.001	< 0.001
Grade IV (n = 19)	Observation 1	0.69 ± 0.15	0.46 ± 0.07	3.11 ± 0.42	0.45 ± 0.10	0.86 ± 0.14	0.76 ± 0.04
	Observation 2	0.66 ± 0.15	0.46 ± 0.07	3.10 ± 0.42	0.45 ± 0.10	0.89 ± 0.16	0.77 ± 0.05
	ICC	0.972	0.991	0.970	0.989	0.799	0.983
	p value	< 0.001	< 0.001	< 0.001	< 0.001	0.001	< 0.001

ADC (× 10^{-3} mm^2/s), Dslow (× 10^{-3} mm^2/s), Dfast (× 10^{-3} mm^2/s), f (unitless), DDC (× 10^{-3} mm^2/s), α (unitless), ICC = Intra-class Correlation Coefficient.

Table 5. Comparison between groups and among groups

Parameter	Comparison	Test	*p* value
ADC	LGG vs HGG	MWU Test	< 0.001*
	G II vs G III	One-way ANOVA with Bonferroni	0.004*
	G III vs G IV	One-way ANOVA with Bonferroni	0.221 (N. S.)
	G II vs G IV	One-way ANOVA with Bonferroni	< 0.001*
	G II vs G III vs G IV	One-way ANOVA with Bonferroni	< 0.001*
Dslow	LGG vs HGG	t-Test	< 0.001*
	G II vs G III	One-way ANOVA with Bonferroni	0.001
	G III vs G IV	One-way ANOVA with Bonferroni	0.047 (N. S.)
	G II vs G IV	One-way ANOVA with Bonferroni	< 0.001*
	G II vs G III vs G IV	One-way ANOVA with Bonferroni	< 0.001*
Dfast	LGG vs HGG	t-Test	< 0.001*
	G II vs G III	One-way ANOVA with Bonferroni	0.089 (N. S.)
	G III vs G IV	One-way ANOVA with Bonferroni	0.027 (N. S.)
	G II vs G IV	One-way ANOVA with Bonferroni	< 0.001*
	G II vs G III vs G IV	One-way ANOVA with Bonferroni	< 0.001*
f	LGG vs HGG	t-Test	< 0.001*
	G II vs G III	One-way ANOVA with Bonferroni	0.005*
	G III vs G IV	One-way ANOVA with Bonferroni	0.020 (N. S.)
	G II vs G IV	One-way ANOVA with Bonferroni	< 0.001*
	G II vs G III vs G IV	One-way ANOVA with Bonferroni	< 0.001*
DDC	LGG vs HGG	MWU Test	< 0.001*
	G II vs G III	One-way ANOVA with Bonferroni	< 0.001*
	G III vs G IV	One-way ANOVA with Bonferroni	0.347 (N. S.)
	G II vs G IV	One-way ANOVA with Bonferroni	< 0.001*
	G II vs G III vs G IV	One-way ANOVA with Bonferroni	< 0.001*
α	LGG vs HGG	t-Test	< 0.001*
	G II vs G III	One-way ANOVA with Bonferroni	< 0.001*
	G III vs G IV	One-way ANOVA with Bonferroni	0.017 (N. S.)
	G II vs G IV	One-way ANOVA with Bonferroni	< 0.001*
	G II vs G III vs G IV	One-way ANOVA with Bonferroni	< 0.001*

ADC (× 10^{-3} mm^2/s), Dslow (× 10^{-3} mm^2/s), Dfast (× 10^{-3} mm^2/s), f (unitless), DDC (× 10^{-3} mm^2/s), α (unitless), *indicates significant, N.S. = Not Significant, MWU = Mann-Whitney U.

Results

Analysis of reliability

The Intra-class Correlation Coefficients of ADC, Dslow, Dfast, f, DDC, and α were found higher than 0.75 (all P < 0.05), which suggested very good measurement reliability of the parameters as illustrated in **Table 4**.

Tests of normality

The parameters Dslow, Dfast, f and, α in the LGG group while all the parameters ADC, Dslow, Dfast, f, DDC, and α in the HGG group demonstrated normal distribution. Moreover, ADC, and DDC in the LGG were found to have non-normal distribution.

Comparison between two groups and among groups

Highly significant differences were found between LGG and HGG for all the parameters (all P < 0.001) (**Table 5**; **Figure 2**). Similarly, all the parameters demonstrated highly significant differences in co-

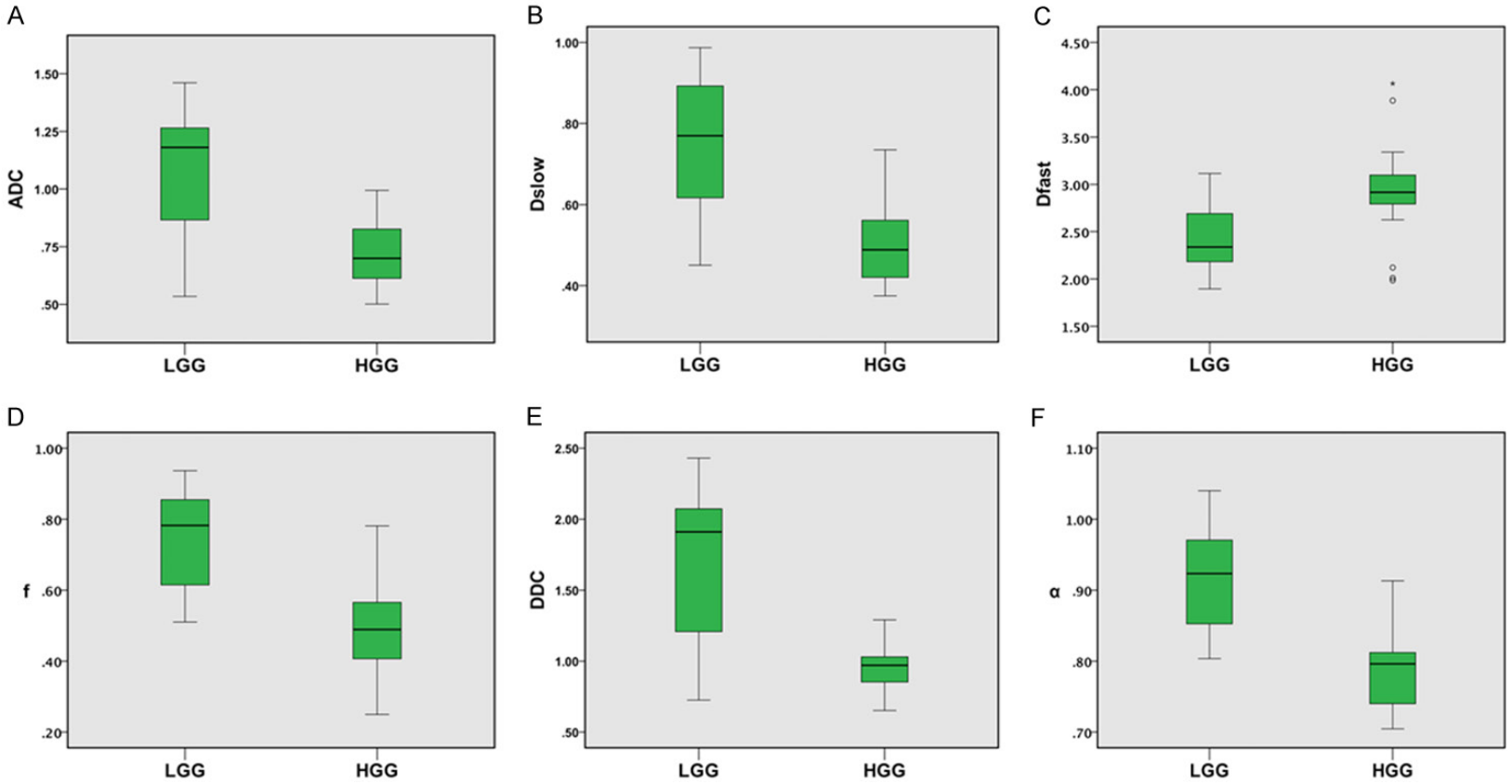

Figure 2. Box plots of the parameters in low and high grade gliomas. 25th, 50th (median), 75th percentiles, minimum, maximum, and outliers of the parameters (A) ADC, (B) Dslow, (C) Dfast, (D) f, (E) DDC, and (F) α. All the parameters are significantly lower in HGG ($P < 0.001$) except Dfast which is significantly higher in HGG ($P < 0.001$). ADC ($\times 10^{-3}$ mm^2/s), Dslow ($\times 10^{-3}$ mm^2/s), Dfast ($\times 10^{-3}$ mm^2/s), f (unitless), DDC ($\times 10^{-3}$ mm^2/s), α (unitless).

Table 6. Correlation of Ki-67 LI with the parameters

		ADC	D slow	D fast	f	DDC	α
Ki-67 LI	Spearman's rho (r)	-0.586	-0.662	0.420	-0.595	-0.608	-0.644
	p value	< 0.001	< 0.001	0.002	< 0.001	< 0.001	< 0.001

ADC (× 10^{-3} mm^2/s), Dslow (× 10^{-3} mm^2/s), Dfast (× 10^{-3} mm^2/s), f (unitless), DDC (× 10^{-3} mm^2/s), α (unitless), Ki-67 LI (%).

mparison among Grade II versus Grade III versus Grade IV gliomas (all P < 0.001). In comparison of Grade II versus Grade III, only ADC, Dslow, f, DDC and α showed significant differences with *p* values of 0.004, 0.001, 0.005, < 0.001, and < 0.001 respectively. All the parameters had no significant differences (all P > 0.0125) in Grade III versus Grade IV while all demonstrated high significant differences in Grade II versus Grade IV (all P < 0.001). The results are presented in **Table 5**.

Correlation of parameters with Ki-67 LI

The parameters ADC, Dslow, Dfast, f, DDC, and α showed moderate to good negative correlation with Ki-67 LI (r = 0.4 to 0.75; P < 0.001 for all), while Dfast (r = 0.420, P = 0.002) also demonstrated moderate to good positive correlation as depicted in **Table 6**; **Figure 3**.

ROC curve analysis

In discriminating high with low grade gliomas, AUC values in descending order were 0.955 for Ki-67 LI; 0.926 for α; 0.903 for Dslow; 0.897 for f; 0.863 for DDC; 0.852 for ADC; 0.820 for Dfast (P < 0.001 for all) which implies diagnostic performance in differentiating between HGG and LGG in the same order (**Figure 4**). The corresponding cut off value, sensitivity and specificity were as depicted in **Table 7**.

Figures 5A-I, **6A-I** display (A) Contrast enhanced-T1WI, (B) DWI at b = 4500 s/mm^2, (C) The ADC map, (D) The Dslow map, (E) The Dfast map, (F) The f map, (G) The DDC map, (H) The α map, and (I) Ki-67 image (400 × magnification) of representative low grade and high grade glioma respectively.

Discussion

The conventional diffusion parameter, ADC has been well established to demonstrate the difference between LGG and HGG, as the tumor parts have increased cellularity and the diffusion gets hindered due to increase in the number of cells resulting in decrease in ADC. However, this fact alone should not be considered because HGG are also associated with increase in vascularity which should result in increase in perfusion related diffusion, and when considered together the increase in both cellularity and vascularity, there should not have been decrease in ADC. In order to explain this contradiction, the use of high b values is required since both perfusion and diffusion derived parameters can be obtained at high b values. Moreover, ADC is not able to fully explain the decrease in diffusion in tumor tissues as the water diffusion deviates from the Gaussian behavior at high b values. Therefore, parameters obtained from biexponential model were evaluated by using high b values as there could be perfusion related parameter affecting the diffusion. However, biexponential model could also be oversimplification of the actual diffusion as there could be potentially more than two pools or compartments (fast and slow) in the tissues. Stretched exponential model which considers the weighted total of any number of compartments over a distribution of ADCs with multiexponential decays, thus was also evaluated.

This study demonstrated that all the parameters had significant discriminating ability between HGG and LGG (P < 0.001 for all) (**Table 5**; **Figure 2A-F**), and the highest diagnostic performance is shown by the parameter α (AUC 0.926, P < 0.001, sensitivity 95.50% and specificity 70.00%) followed by Dslow (AUC 0.903, P < 0.001, sensitivity 87.10% and specificity 80.00%); f (AUC 0.897, P < 0.001, sensitivity 83.90% and specificity 80.00%); DDC (AUC 0.863, P < 0.001, sensitivity 100.00% and specificity 75.00%); ADC (AUC 0.852 P < 0.001, sensitivity 67.70% and specificity 90.00%); Dfast (AUC 0.820 P < 0.001, sensitivity 80.00% and specificity 87.10%) in differentiating HGG from LGG (**Table 7**; **Figure 4A** and **4B**). The α value which is water diffusion heterogeneity index ranges from 0 to 1. According to the stretched exponential model

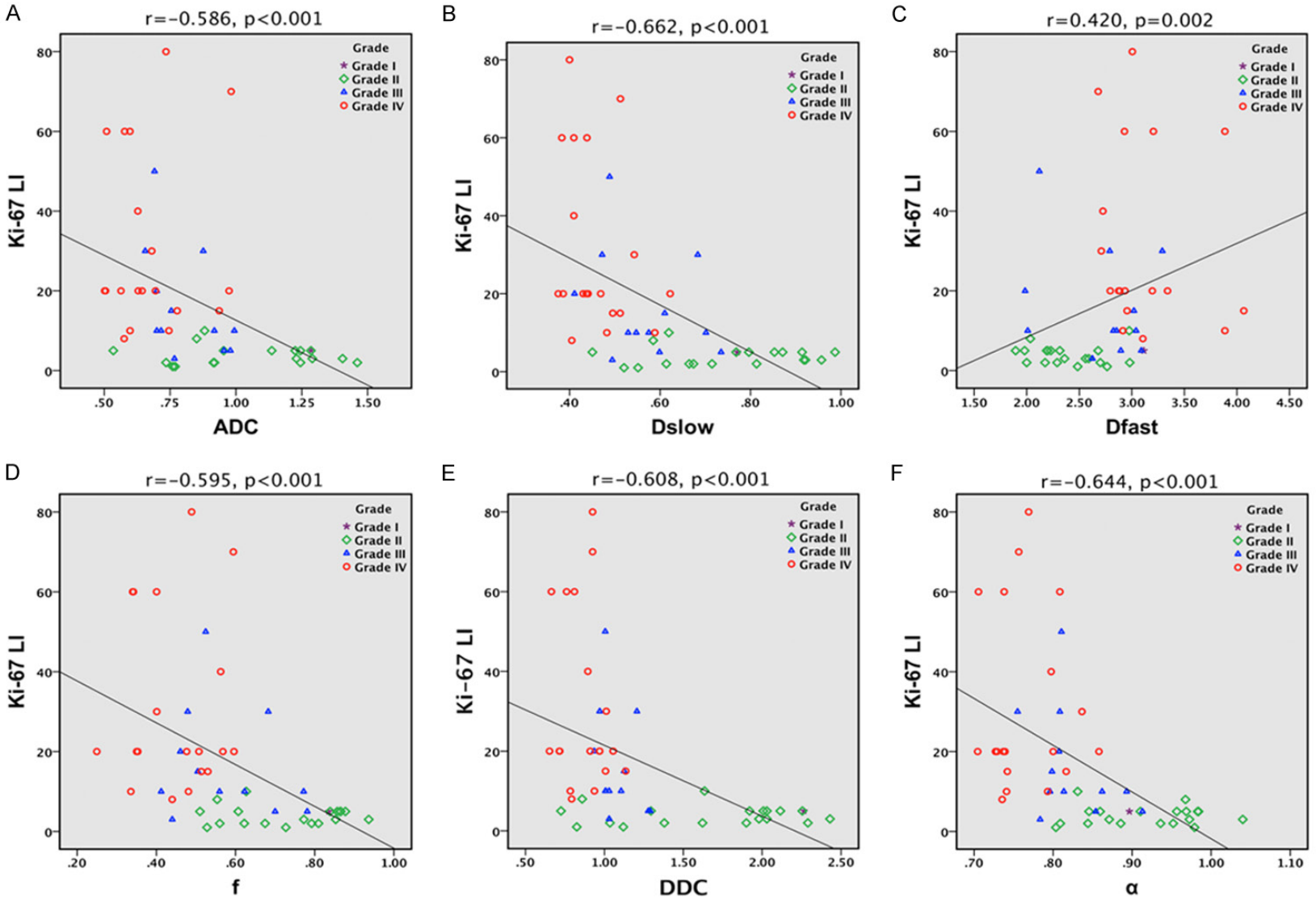

Figure 3. Scatter plots of the parameters with correlation to Ki-67 LI. (A) ADC, (B) Dslow, (C) Dfast, (D) f, (E) DDC, and (F) α. ADC, Dslow, Dfast, f, DDC, and α show moderate to good negative correlation with Ki-67 LI (r = 0.4 to 0.75; P < 0.001 for all), while Dfast (r = 0.420, P = 0.002) demonstrate moderate to good positive correlation. ADC (× 10^{-3} mm^2/s), Dslow (× 10^{-3} mm^2/s), Dfast (× 10^{-3} mm^2/s), f (unitless), DDC (× 10^{-3} mm^2/s), α (unitless).

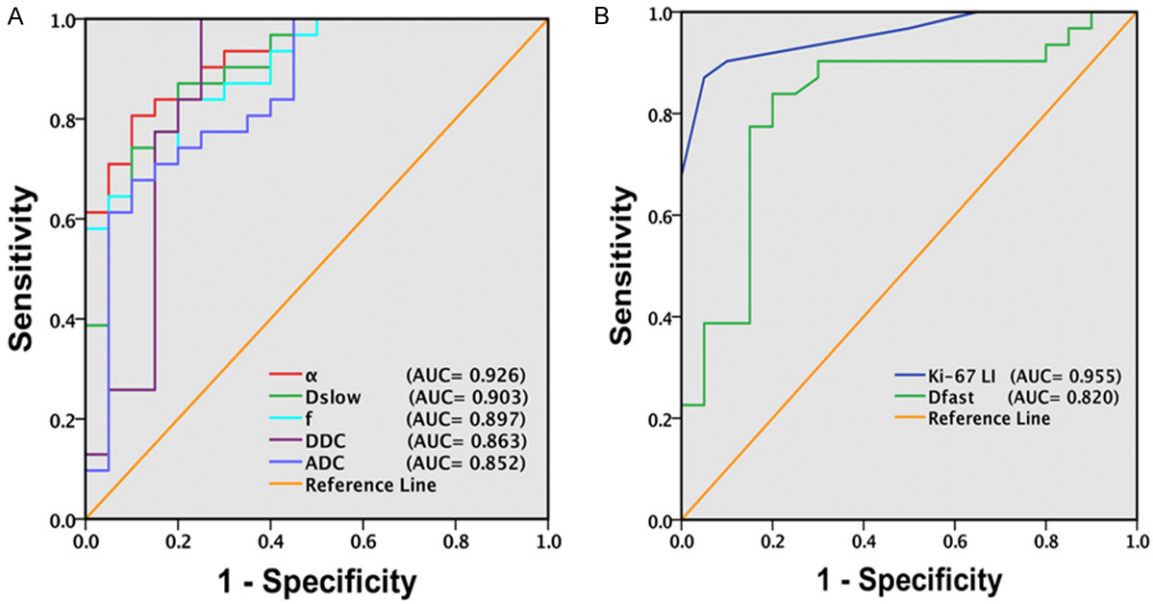

Figure 4. ROC curve in differentiating high versus low grade gliomas by the parameters. A. Diagnostic performance of ADC, Dslow, f, DDC, and α; B. Diagnostic performance of Ki-67 LI and Dfast in differentiating HGG from LGG. AUC values in descending order were 0.955 for Ki-67 LI, 0.926 for α, 0.903 for Dslow, 0.897 for f, 0.863 for DDC, 0.852 for ADC, and 0.820 for Dfast (P < 0.001 for all) which implies diagnostic performance in the same order. ADC (× 10^{-3} mm^2/s), Dslow (× 10^{-3} mm^2/s), Dfast (× 10^{-3} mm^2/s), f (unitless), DDC (× 10^{-3} mm^2/s), α (unitless), Ki-67 LI (%), AUC = Area Under ROC Curve.

Table 7. Diagnostic performance of the parameters by ROC curve

	AUC (95% CI)	*p*-value	Youden index	Cut-off value	Sensitivity (%)	Specificity (%)
ADC	0.852 (0.739-0.964)	< 0.001	0.577	0.757	67.70	90.00
Dslow	0.903 (0.820-0.987)	< 0.001	0.671	0.612	87.10	80.00
f	0.897 (0.815-0.979)	< 0.001	0.639	0.601	83.90	80.00
DDC	0.863 (0.737-0.989)	< 0.001	0.750	1.292	100.00	75.00
α	0.926 (0.858-0.993)	< 0.001	0.635	0.866	93.50	70.00
Dfast	0.820 (0.695-0.946)	< 0.001	0.639	2.705	80.00	87.10
Ki-67 LI	0.955 (0.903-1.000)	< 0.001	0.821	9.000	95.00	87.10

ADC (× 10^{-3} mm^2/s), Dslow (× 10^{-3} mm^2/s), Dfast (× 10^{-3} mm^2/s), f (unitless), DDC (× 10^{-3} mm^2/s), α (unitless), Ki-67 LI (%), 95% CI = 95% Confidence Interval.

Equation 3 described above, as α value approaches 1, DDC equals ADC and conversely, as its value tends to approach 0, DDC is very less than the ADC. Thus, the heterogeneity in diffusion could well be positively related to the heterogeneity and complexity of the HGG. Moreover, α was found to have good negative correlation with Ki-67 LI (r = -0.608, P < 0.001) (**Table 6**; **Figure 3F**). Previous studies also report high diagnostic efficacy of α [21, 29]. Similarly, DDC (AUC 0.863, P < 0.001) derived from stretched exponential model was also found useful than ADC (AUC 0.852, P < 0.001) but less than that of α, Dslow and f (**Table 7**; **Figure 4A**), which is in consistent with previous studies [21, 29]. This could be because the difference in DDC between HGG and LGG may become less obvious at high b values since a large number of low b values contribute to DDC according to the fitting function [30], and additionally there is negative correlation between DDC and alpha (α) in HGG [31].

In the current study, the biexponential derived parameter Dslow was significantly lower in HGG (0.50 ± 0.10) than LGG (0.75 ± 0.16) and showed significant difference between HGG and LGG (P < 0.001) (**Tables 2**, **5**; **Figure 2B**),

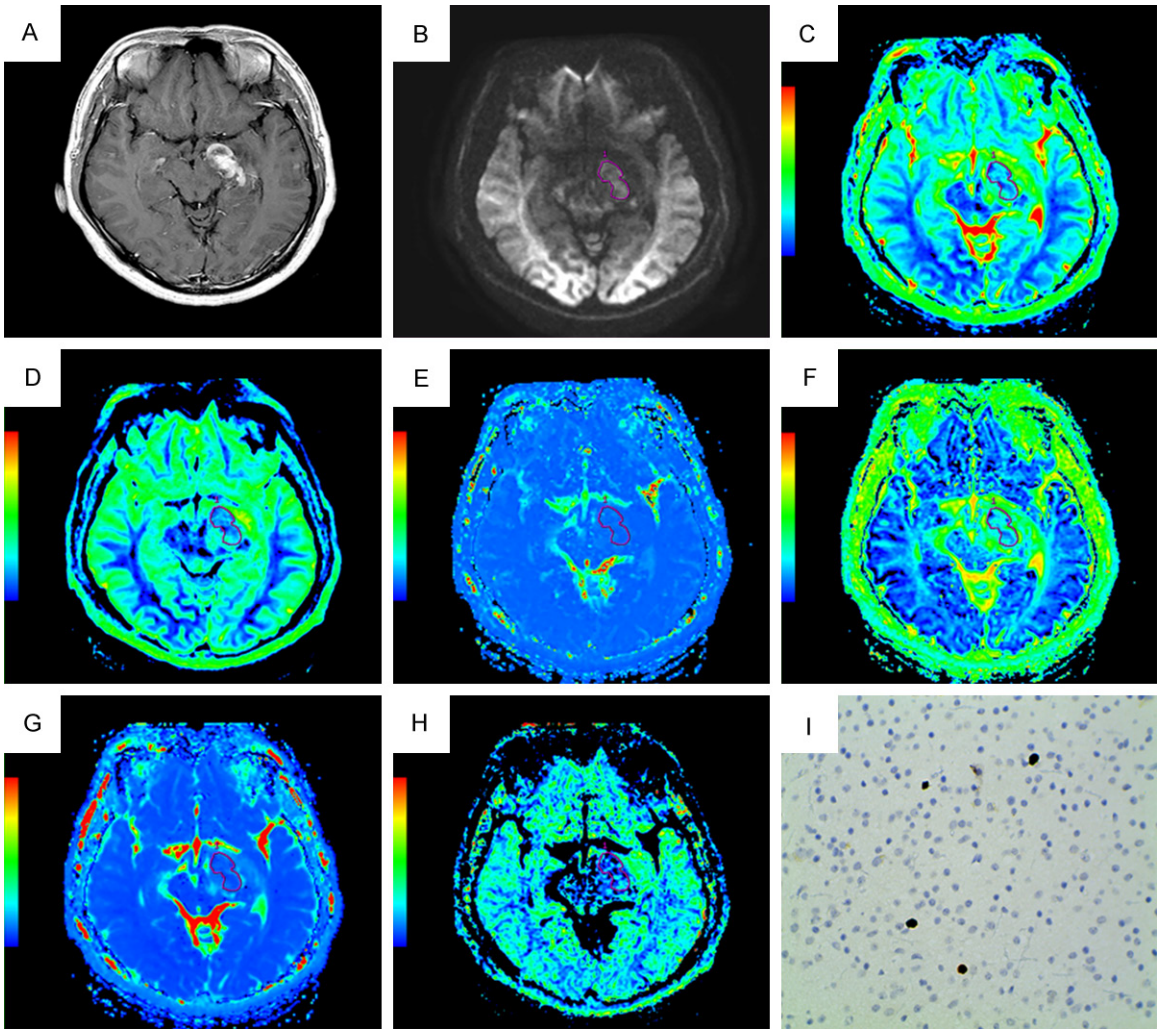

Figure 5. A non-homogeneously enhancing low grade glioma (WHO Grade II) in a 26-year-old male in left temporal region. (A) Contrast enhanced-T1WI, (B) DWI at b = 4500 s/mm^2, (C) The ADC map, (D) The Dslow map, (E) The Dfast map, (F) The f map, (G) The DDC map, (H) The α map, and (I) Ki-67 image (400 × magnification). DWI shows increased signal intensity; the functional maps of ADC, Dslow, f, DDC and α show predominantly decreased signal values; the Dfast map shows predominantly increased signal value encoded in a green-yellow-red color schema in increasing value order. The Ki-67 LI value was 2%.

and also showed better performance than conventional model derived parameter ADC (**Table 7**; **Figure 4A**). These findings are in agreement with prior studies [21, 29, 32-34]. At low b values, according to the biexponential model, the diffusion mostly reflects from the extracellular space which is perfusion related information but at high values intracellular component of diffusion can be obtained which is required in cases of increased cellularity like in HGG which could be possible reason for the inconsistency from the previous study that used low b values. Dslow also demonstrated the strongest negative correlation with the Ki-67 LI (r = -0.662, P < 0.001) (**Table 6**; **Figure 3B**). This again is the supporting evidence that Dslow provides information of increased cellular proliferation. Another biexponential model derived parameter f was also found to be significantly lower in HGG than LGG (HGG: 0.50 ± 0.13; LGG: 0.74 ± 0.14; P < 0.001) (**Tables 2**, **5**; **Figure 2D**), which is in agreement with other studies [29, 32, 35]. However, several other studies have found higher f in HGG [33, 34, 36]. Although theoretically higher values of f are expected as it represents volume fraction of rapid diffusion component in a voxel reflecting perfusion of the tissue, the contradiction of this study could be

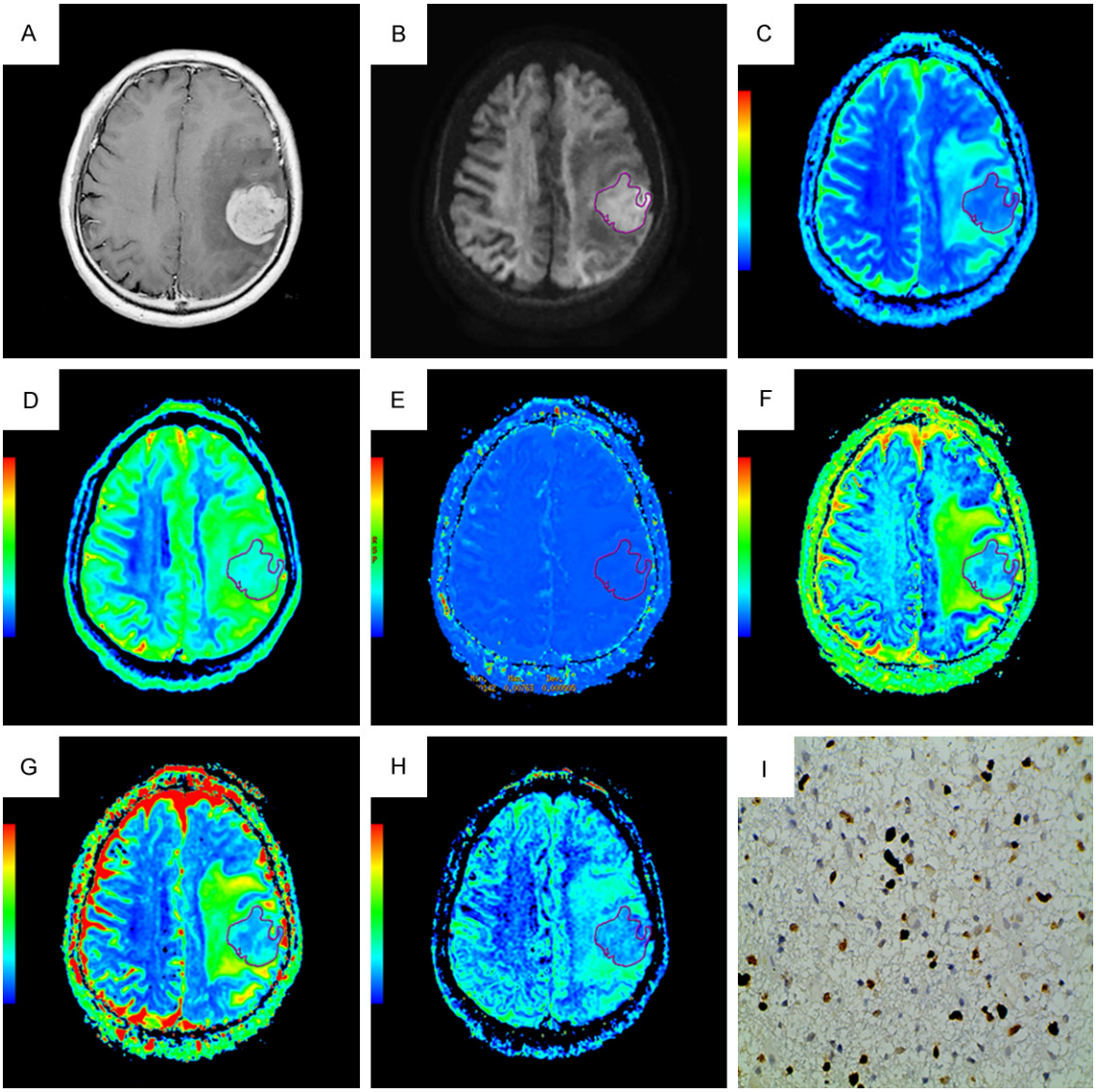

Figure 6. A homogeneously enhancing high grade glioma (WHO Grade IV) in a 60-year-old male in left frontal region. (A) Contrast enhanced-T1WI, (B) DWI at b = 4500 s/mm^2, (C) The ADC map, (D) The Dslow map, (E) The Dfast map, (F) The f map, (G) The DDC map, (H) The α map, and (I) Ki-67 image (400 × magnification). DWI shows increased signal intensity; the functional maps of ADC, Dslow, f, DDC and α show predominantly decreased signal values; the Dfast map shows predominantly increased signal values encoded in a green-yellow-red color schema in increasing value order. The Ki-67 LI was 40%.

because of difference in selection of tumor cases and their structural variation and selection of different b value range by other studies, since low b values are more valuable for pseudo-diffusion calculation [37]. However, the average f value of white matter was found higher than that of LGG [34], and the higher cellular density and nuclear to cytoplasmic ratio with fewer mesenchymal structures as reported by other studies might be the cause lower f value in HGG [36, 38]. Dfast was found to be significantly higher in HGG (2.95 ± 0.46) than LGG (2.43 ± 0.36), P < 0.001 (**Tables 2**, **5**; **Figure 2C**), which is in consistent with other studies [29, 32, 34, 35], which could reflect the amount of neovascularization and micro-vessel density in HGG which is related to an average length of capillaries and blood flow velocities [39].

However, inconsistent results were observed among between group comparisons (Grade II vs Grade III, Grade III vs Grade IV, and Grade II

vs Grade IV) when compared with other study [21] as demonstrated in **Table 5**. In comparison of Grade II versus Grade III, only ADC, Dslow, f, DDC and α showed significant differences with *p* values of 0.004, 0.001, 0.005, < 0.001, and < 0.001 respectively. All the parameters had no significant differences (all P > 0.125) in Grade III versus Grade IV while all demonstrated high significant differences in Grade II versus Grade IV (all P < 0.001). The possible reason for this disparity could be the limitation of this study that Grade II consisted of few patients (n = 12) which could have resulted in the non-significant difference while comparison between groups of Grade II versus Grade III, and Grade II versus Grade IV. This study had some other limitations also. Sampling bias might have occurred due to retrospective selection of the patients. The molecular information according to 2016 WHO updated classification was not evaluated in our study, thus future studies need to assess relationship between molecular and MRI parameters.

To conclude, in comparison to ADC derived from monoexponential model, the parameters α and Dslow derived from stretched exponential, and biexponential models respectively can efficiently differentiate HGG from LGG with high diagnostic accuracy. Additionally, f and DDC derived from biexponential, and stretched exponential models respectively are also more useful in differentiating HGG from LGG in comparison to ADC.

Acknowledgements

This work was supported by grants from the National Natural Science Foundation of China (No. 81570462, No. 81730049, No. 81801666, No. 81171308, and No. 81401389).

Disclosure of conflict of interest

None.

Address correspondence to: Dr. Wenzhen Zhu, Department of Radiology, Tongji Hospital, No. 1095 Jiefang Avenue, Wuhan 430030, Hubei, China. Tel: +86-02783663258; Fax: +86-02783663258; E-mail: zhuwenzhen8612@163.com

References

[1] Louis DN, Ohgaki H, Wiestler OD, Cavenee WK, Burger PC, Jouvet A, Scheithauer BW and Kleihues P. The 2007 WHO classification of tumours of the central nervous system. Acta Neuropathol 2007; 114: 97-109.

[2] Louis DN, Perry A, Reifenberger G, von Deimling A, Figarella-Branger D, Cavenee WK, Ohgaki H, Wiestler OD, Kleihues P and Ellison DW. The 2016 World Health Organization classification of tumors of the central nervous system: a summary. Acta Neuropathol 2016; 131: 803-820.

[3] Johnson DR, Guerin JB, Giannini C, Morris JM, Eckel LJ and Kaufmann TJ. 2016 updates to the WHO brain tumor classification system: what the radiologist needs to know. Radiographics 2017; 37: 2164-2180.

[4] Ganau L, Paris M, Ligarotti GK and Ganau M. Management of gliomas: overview of the latest technological advancements and related behavioral drawbacks. Behav Neurol 2015; 2015: 862634.

[5] Nitta M, Muragaki Y, Maruyama T, Ikuta S, Komori T, Maebayashi K, Iseki H, Tamura M, Saito T, Okamoto S, Chernov M, Hayashi M and Okada Y. Proposed therapeutic strategy for adult low-grade glioma based on aggressive tumor resection. Neurosurg Focus 2015; 38: E7.

[6] Khan MN, Sharma AM, Pitz M, Loewen SK, Quon H, Poulin A and Essig M. High-grade glioma management and response assessment-recent advances and current challenges. Curr Oncol 2016; 23: e383-391.

[7] Bush NA, Chang SM and Berger MS. Current and future strategies for treatment of glioma. Neurosurg Rev 2017; 40: 1-14.

[8] Furnari FB, Fenton T, Bachoo RM, Mukasa A, Stommel JM, Stegh A, Hahn WC, Ligon KL, Louis DN, Brennan C, Chin L, DePinho RA and Cavenee WK. Malignant astrocytic glioma: genetics, biology, and paths to treatment. Genes Dev 2007; 21: 2683-2710.

[9] Kao HW, Chiang SW, Chung HW, Tsai FY and Chen CY. Advanced MR imaging of gliomas: an update. Biomed Res Int 2013; 2013: 970586.

[10] Skjulsvik AJ, Mork JN, Torp MO and Torp SH. Ki-67/MIB-1 immunostaining in a cohort of human gliomas. Int J Clin Exp Pathol 2014; 7: 8905-8910.

[11] Thotakura M, Tirumalasetti N and Krishna R. Role of Ki-67 labeling index as an adjunct to the histopathological diagnosis and grading of astrocytomas. J Cancer Res Ther 2014; 10: 641-645.

[12] Perry A and Wesseling P. Histologic classification of gliomas. Handb Clin Neurol 2016; 134: 71-95.

[13] Alexiou GA, Tsiouris S, Kyritsis AP, Argyropoulou MI, Voulgaris S and Fotopoulos AD. Assessment of glioma proliferation using imaging modalities. J Clin Neurosci 2010; 17: 1233-1238.

[14] Hagmann P, Jonasson L, Maeder P, Thiran JP, Wedeen VJ and Meuli R. Understanding diffusion MR imaging techniques: from scalar diffusion-weighted imaging to diffusion tensor imaging and beyond. Radiographics 2006; 26 Suppl 1: S205-223.
[15] Schaefer PW, Grant PE and Gonzalez RG. Diffusion-weighted MR imaging of the brain. Radiology 2000; 217: 331-345.
[16] Le Bihan D, Breton E, Lallemand D, Grenier P, Cabanis E and Laval-Jeantet M. MR imaging of intravoxel incoherent motions: application to diffusion and perfusion in neurologic disorders. Radiology 1986; 161: 401-407.
[17] Bennett KM, Schmainda KM, Bennett RT, Rowe DB, Lu H and Hyde JS. Characterization of continuously distributed cortical water diffusion rates with a stretched-exponential model. Magn Reson Med 2003; 50: 727-734.
[18] Le Bihan D, Breton E, Lallemand D, Aubin ML, Vignaud J and Laval-Jeantet M. Separation of diffusion and perfusion in intravoxel incoherent motion MR imaging. Radiology 1988; 168: 497-505.
[19] Iima M and Le Bihan D. Clinical intravoxel incoherent motion and diffusion mr imaging: past, present, and future. Radiology 2016; 278: 13-32.
[20] Bennett KM, Hyde JS, Rand SD, Bennett R, Krouwer HG, Rebro KJ and Schmainda KM. Intravoxel distribution of DWI decay rates reveals C6 glioma invasion in rat brain. Magn Reson Med 2004; 52: 994-1004.
[21] Yan R, Haopeng P, Xiaoyuan F, Jinsong W, Jiawen Z, Chengjun Y, Tianming Q, Ji X, Mao S, Yueyue D, Yong Z, Jianfeng L and Zhenwei Y. Non-Gaussian diffusion MR imaging of glioma: comparisons of multiple diffusion parameters and correlation with histologic grade and MIB-1 (Ki-67 labeling) index. Neuroradiology 2016; 58: 121-132.
[22] Jiang R, Jiang J, Zhao L, Zhang J, Zhang S, Yao Y, Yang S, Shi J, Shen N, Su C, Zhang J and Zhu W. Diffusion kurtosis imaging can efficiently assess the glioma grade and cellular proliferation. Oncotarget 2015; 6: 42380-42393.
[23] Johannessen AL and Torp SH. The clinical value of Ki-67/MIB-1 labeling index in human astrocytomas. Pathol Oncol Res 2006; 12: 143-147.
[24] Ambroise MM, Khosla C, Ghosh M, Mallikarjuna VS and Annapurneswari S. Practical value of MIB-1 index in predicting behavior of astrocytomas. Indian J Pathol Microbiol 2011; 54: 520-525.
[25] Alexiou GA, Zikou A, Tsiouris S, Goussia A, Kosta P, Papadopoulos A, Voulgaris S, Kyritsis AP, Fotopoulos AD and Argyropoulou MI. Correlation of diffusion tensor, dynamic susceptibility contrast MRI and (99m)Tc-Tetrofosmin brain SPECT with tumour grade and Ki-67 immunohistochemistry in glioma. Clin Neurol Neurosurg 2014; 116: 41-45.
[26] Tao H, Li H, Hua Y, Chen Z, Feng X and Chen S. Quantitative magnetic resonance imaging (MRI) evaluation of cartilage repair after microfracture treatment for full-thickness cartilage defect models in rabbit knee joints: correlations with histological findings. Skeletal Radiol 2015; 44: 393-402.
[27] Woo S, Lee JM, Yoon JH, Joo I, Han JK and Choi BI. Intravoxel incoherent motion diffusion-weighted MR imaging of hepatocellular carcinoma: correlation with enhancement degree and histologic grade. Radiology 2014; 270: 758-767.
[28] Youden WJ. Index for rating diagnostic tests. Cancer 1950; 3: 32-35.
[29] Bai Y, Lin Y, Tian J, Shi D, Cheng J, Haacke EM, Hong X, Ma B, Zhou J and Wang M. Grading of gliomas by using monoexponential, biexponential, and stretched exponential diffusion-weighted mr imaging and diffusion kurtosis MR imaging. Radiology 2016; 278: 496-504.
[30] Kwee TC, Galban CJ, Tsien C, Junck L, Sundgren PC, Ivancevic MK, Johnson TD, Meyer CR, Rehemtulla A, Ross BD and Chenevert TL. Comparison of apparent diffusion coefficients and distributed diffusion coefficients in high-grade gliomas. J Magn Reson Imaging 2010; 31: 531-537.
[31] Kwee TC, Galban CJ, Tsien C, Junck L, Sundgren PC, Ivancevic MK, Johnson TD, Meyer CR, Rehemtulla A, Ross BD and Chenevert TL. Intravoxel water diffusion heterogeneity imaging of human high-grade gliomas. NMR Biomed 2010; 23: 179-187.
[32] Hu YC, Yan LF, Wu L, Du P, Chen BY, Wang L, Wang SM, Han Y, Tian Q, Yu Y, Xu TY, Wang W and Cui GB. Intravoxel incoherent motion diffusion-weighted MR imaging of gliomas: efficacy in preoperative grading. Sci Rep 2014; 4: 7208.
[33] Togao O, Hiwatashi A, Yamashita K, Kikuchi K, Mizoguchi M, Yoshimoto K, Suzuki SO, Iwaki T, Obara M, Van Cauteren M and Honda H. Differentiation of high-grade and low-grade diffuse gliomas by intravoxel incoherent motion MR imaging. Neuro Oncol 2016; 18: 132-141.
[34] Bisdas S, Koh TS, Roder C, Braun C, Schittenhelm J, Ernemann U and Klose U. Intravoxel incoherent motion diffusion-weighted MR imaging of gliomas: feasibility of the method and initial results. Neuroradiology 2013; 55: 1189-1196.
[35] Lin Y, Li J, Zhang Z, Xu Q, Zhou Z, Zhang Z, Zhang Y and Zhang Z. Comparison of intravoxel incoherent motion diffusion-weighted MR

imaging and arterial spin labeling MR imaging in gliomas. Biomed Res Int 2015; 2015: 234245.

[36] Federau C, Meuli R, O'Brien K, Maeder P and Hagmann P. Perfusion measurement in brain gliomas with intravoxel incoherent motion MRI. AJNR Am J Neuroradiol 2014; 35: 256-262.

[37] Cohen AD, Schieke MC, Hohenwalter MD and Schmainda KM. The effect of low b-values on the intravoxel incoherent motion derived pseudodiffusion parameter in liver. Magn Reson Med 2015; 73: 306-311.

[38] Hu LS, Eschbacher JM, Dueck AC, Heiserman JE, Liu S, Karis JP, Smith KA, Shapiro WR, Pinnaduwage DS, Coons SW, Nakaji P, Debbins J, Feuerstein BG and Baxter LC. Correlations between perfusion MR imaging cerebral blood volume, microvessel quantification, and clinical outcome using stereotactic analysis in recurrent high-grade glioma. AJNR Am J Neuroradiol 2012; 33: 69-76.

[39] Lee HJ, Rha SY, Chung YE, Shim HS, Kim YJ, Hur J, Hong YJ and Choi BW. Tumor perfusion-related parameter of diffusion-weighted magnetic resonance imaging: correlation with histological microvessel density. Magn Reson Med 2014; 71: 1554-1558.